Dalton Transactions

PAPER

View Article Online
View Journal | View Issue

Cite this: *Dalton Trans.*, 2017, **46**, 9591

Copper(II) complexes of functionalized 2,2′:6′,2″-terpyridines and 2,6-di(thiazol-2-yl)pyridine: structure, spectroscopy, cytotoxicity and catalytic activity†

Katarzyna Czerwińska, [a] Barbara Machura, *[a] Slawomir Kula, [b] Stanisław Krompiec,[b] Karol Erfurt,[c] Catarina Roma-Rodrigues,[d] Alexandra R. Fernandes,*[d] Lidia S. Shul'pina, [e] Nikolay S. Ikonnikov[e] and Georgiy B. Shul'pin *[f,g]

Six new copper(II) complexes with 2,2′:6′,2″-terpyridine (4′-R^n-terpy) [**1** (R^1 = furan-2-yl), **2** (R^2 = thiophen-2-yl), and **3** (R^3 = 1-methyl-1*H*-pyrrol-2-yl)] and 2,6-di(thiazol-2-yl)pyridine derivatives (R^n-dtpy) [**4** (R^1), **5** (R^2), and **6** (R^3)] have been synthesized by a reaction between copper(II) chloride and the corresponding ligand. The complexes have been characterized by UV-vis and IR spectroscopy, and their structures have been determined by X-ray analysis. The antiproliferative potential of copper(II) complexes of 2,2′:6′,2″-terpyridine and 2,6-di(thiazol-2-yl)pyridine derivatives towards human colorectal (HCT116) and ovarian (A2780) carcinoma as well as towards lung (A549) and breast adenocarcinoma (MCF7) cell lines was examined. Complex **1** and complex **6** were found to have the highest antiproliferative effect on A2780 ovarian carcinoma cells, particularly when compared with complex **2**, **3** with no antiproliferative effect. The order of cytotoxicity in this cell line is **6** > **1** > **5** > **4** > **2** ≈ **3**. Complex **2** seems to be much more specific towards colorectal carcinoma HCT116 and lung adenocarcinoma A549 cells. The viability loss induced by the complexes agrees with Hoechst 33258 staining and typical morphological apoptotic characteristics like chromatin condensation and nuclear fragmentation. The specificity towards different types of cell lines and the low cytotoxic activity towards healthy cells are of particular interest and are a positive feature for further developments. Complexes **1–6** were also tested in the oxidation of alkanes and alcohols with hydrogen peroxide and *tert*-butyl-hydroperoxide (TBHP). The most active catalyst **4** gave, after 120 min, 0.105 M of cyclohexanol + cyclohexanone after reduction with PPh_3. This concentration corresponds to a yield of 23% and TON = 210. Oxidation of *cis*-1,2-dimethylcyclohexane with *m*-CPBA catalyzed by **4** in the presence of HNO_3 gave a product of a stereoselective reaction (*trans*/*cis* = 0.47). Oxidation of secondary alcohols afforded the target ketones in yields up to 98% and TON = 630.

Received 6th April 2017,
Accepted 23rd June 2017

DOI: 10.1039/c7dt01244f

rsc.li/dalton

Introduction

Transition metal complexes of 4′-functionalized 2,2′:6′,2″-terpyridines have attracted widespread scientific attention in view of their interesting electronic, photonic, magnetic, reactive and structural properties,[1] as well as promising applications in catalysis,[2] molecular magnetism,[3] molecular electronics,[4] supramolecular chemistry[5] and anti-tumor therapy.[6]

[a]*Department of Crystallography, Institute of Chemistry, University of Silesia, 9th Szkolna St, 40-006 Katowice, Poland. E-mail: bmachura@poczta.onet.pl*
[b]*Department of Inorganic, Organometallic Chemistry and Catalysis, Institute of Chemistry, University of Silesia, 9th Szkolna St, 40-006 Katowice, Poland*
[c]*Department of Chemical Organic Technology and Petrochemistry, Silesian University of Technology, Krzywoustego 4, 44-100 Gliwice, Poland*
[d]*UCIBIO, Departamento de Ciências da Vida, Faculdade de Ciências e Tecnologia, Universidade NOVA de Lisboa, Campus de Caparica, 2829-516 Caparica, Portugal. E-mail: ma.fernandes@fct.unl.pt*
[e]*Nesmeyanov Institute of Organoelement Compounds, Russian Academy of Sciences, ulitsa Vavilova, dom 28, Moscow 119991, Russia*
[f]*Department of Kinetics and Catalysis, Semenov Institute of Chemical Physics, Russian Academy of Sciences, ulitsa Kosygina, dom 4, Moscow 119991, Russia. E-mail: shulpin@chph.ras.ru*
[g]*Chair of Chemistry and Physics, Plekhanov Russian University of Economics, Stremyannyi pereulok, dom 36, Moscow 117997, Russia*

†Electronic supplementary information (ESI) available: Bond lengths and angles, dihedral angles between aromatic rings, short intra- and intermolecular contacts, electronic absorption spectra in methanol, IR spectra, XPRD patterns, and HRMS results. CCDC 1540061–1540066. For ESI and crystallographic data in CIF or other electronic format see DOI: 10.1039/c7dt01244f

Substituents in 2,2′:6′,2″-terpyridines and 2,6-di(thiazol-2-yl)-pyridines are utilized to tailor the electronic properties of the ligand and its metal complexes, as well as to incorporate new functionalities using further derivatisation reactions. For metal ion based drugs, the ligand nature is of great importance in the binding of the complex to a biomolecule such as DNA or protein. The chelating ability of 2,2′:6′,2″-terpyridine enhances the stability of the metal complex, and planarity of the ligand leads to strong intercalative interaction of the complex with DNA.[7]

In the field of anticancer drug design, special attention has been devoted to copper(II) complexes with 2,2′:6′,2″-terpyridines owing to the bio-essential nature of Cu(II) ions. Studies revealed that these complexes are able to promote the generation of reactive oxygen species (ROS) in the presence of mild reducing agents, which has been exploited to oxidatively break the DNA strands and further to inhibit the proliferation of tumor cells.[8] In the recent past, 2,2′:6′,2″-terpyridine-based copper(II) complexes have also found remarkable applications as catalysts for the aerobic oxidation of alcohols under mild conditions.[9]

Herein, three functionalized 2,2′:6′,2″-terpyridines and three 2,6-di(thiazol-2-yl)pyridines were used to generate copper(II) complexes (Schemes 1 and 2), and their cytotoxicity as well as catalytic activity in the oxidation of alkanes and alcohols were investigated. Interestingly, 2,6-di(thiazol-2-yl)pyridine derivatives, considered to be 2,2′:6′,2″-terpyridine analogues, have received far less attention compared to 2,2′:6′,2″-terpyridine derivatives. Although a thiazole ring is related to pyridine in its aromaticity and general chemistry, it differs in electronic properties. To the best of our knowledge, only a few transition metal complexes of 2,6-di(thiazol-2-yl)pyridines have been reported so far.[10] The known in the literature[11] complex [$CuCl_2$(terpy)] with an unsubstituted terpyridine has been synthesized and investigated here for comparison with other substituted compounds.

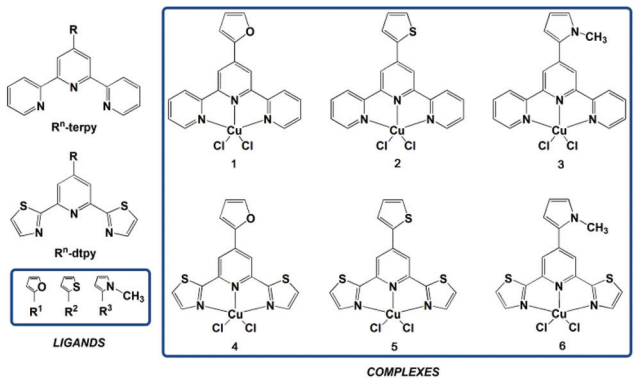

Scheme 1 The substituted 2,2′:6′,2″-terpyridine (R^n-terpy) and 2,6-di(thiazol-2-yl)pyridine (R^n-dtpy) ligands prepared in this work, as well as copper complexes bearing these ligands.

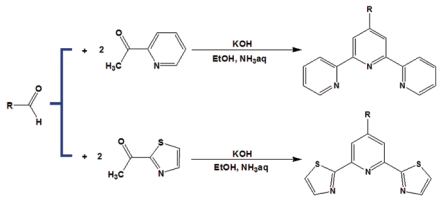

Scheme 2 The synthetic route to 2,2′:6′,2″-terpyridine (R^n-terpy) and 2,6-di(thiazol-2-yl)pyridine derivatives (R^n-dtpy).

Results and discussion

Synthesis and general characterization of the complexes

2,2′:6′,2″-Terpyridine and 2,6-di(thiazol-2-yl)pyridine derivatives were obtained by condensation of the corresponding aldehyde with 2-acetylpyridine and 2-acetylthiazole, respectively, as shown in Scheme 2. The first step of a base-mediated Kröhnke condensation is not isolated, but undergoes *in situ* pyridine ring closure performed in the presence of an ammonia source.[12]

The copper complexes were isolated as green solids by the reaction of a methanol solution of the appropriate ligand with a methanolic solution of $CuCl_2{\cdot}2H_2O$. In the IR spectra, the characteristic bands assignable to ν(C=C) and ν(C=N) vibrations of coordinated N-heterocyclic ligands are observed in the range 1615–1526 cm^{-1} (see Fig. S3 in the ESI†). Compared to the free ligands, they are slightly shifted towards higher wavenumbers.

The electronic reflectance spectra of the examined copper(II) compounds (Fig. 1) are characterized by a very broad asymmetric band in the region 600–1000 nm typical for overlapping $d_{xy} \rightarrow d_{x^2-y^2}$, d_{yz}, $d_{xz} \rightarrow d_{x^2-y^2}$ and $d_{z^2} \rightarrow d_{x^2-y^2}$ transitions between d orbitals of the coordinated copper(II) ion.[13] A collection of bands below 400 nm are attributed to triimine-centred $\pi \rightarrow \pi^*$ and $n \rightarrow \pi^*$ excitations (see also Fig. S2†).

Molecular structures

Perspective views of the asymmetric units of **1–6** are shown in Fig. 2. The selected bond distances and bond angles were included in ESI (Table S2†).

The crystal structure of **1** is composed of mononuclear units [$CuCl_2$(R^1-terpy)] and co-crystallised methanol molecules, while the structure of **3** comprises two independent molecules per asymmetric unit (Fig. 2). The independent complex molecules with Cu(1) and Cu(2) centres are five coordinated by three nitrogen atoms of the tridentate coordinated R^3-terpy molecule and two chloride ions, but they differ noticeably in the geometry around the metal center. The angular structural index parameters τ[14] of 0.077 for molecule **A** and 0.457 for **B** ion indicate that the geometry of the metal centres Cu(1) and Cu(2) may be described as a distorted square-pyramid and an intermediate between a trigonal bipyramid and a square-pyramid, respectively. The distortion of the coordination sphere of Cu(1) and Cu(2) ions in **3** from ideal five-vertex polyhedra (square-pyramid and trigonal bipyramid) was also calcu-

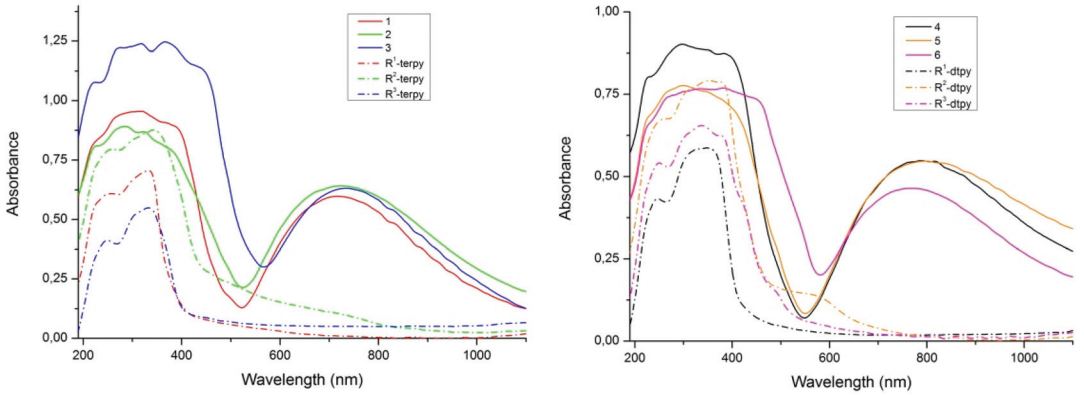

Fig. 1 The solid state absorption UV-Vis spectra of the free ligands (R^n-terpy and R^n-dtpy) and Cu(II) complexes (**1–6**).

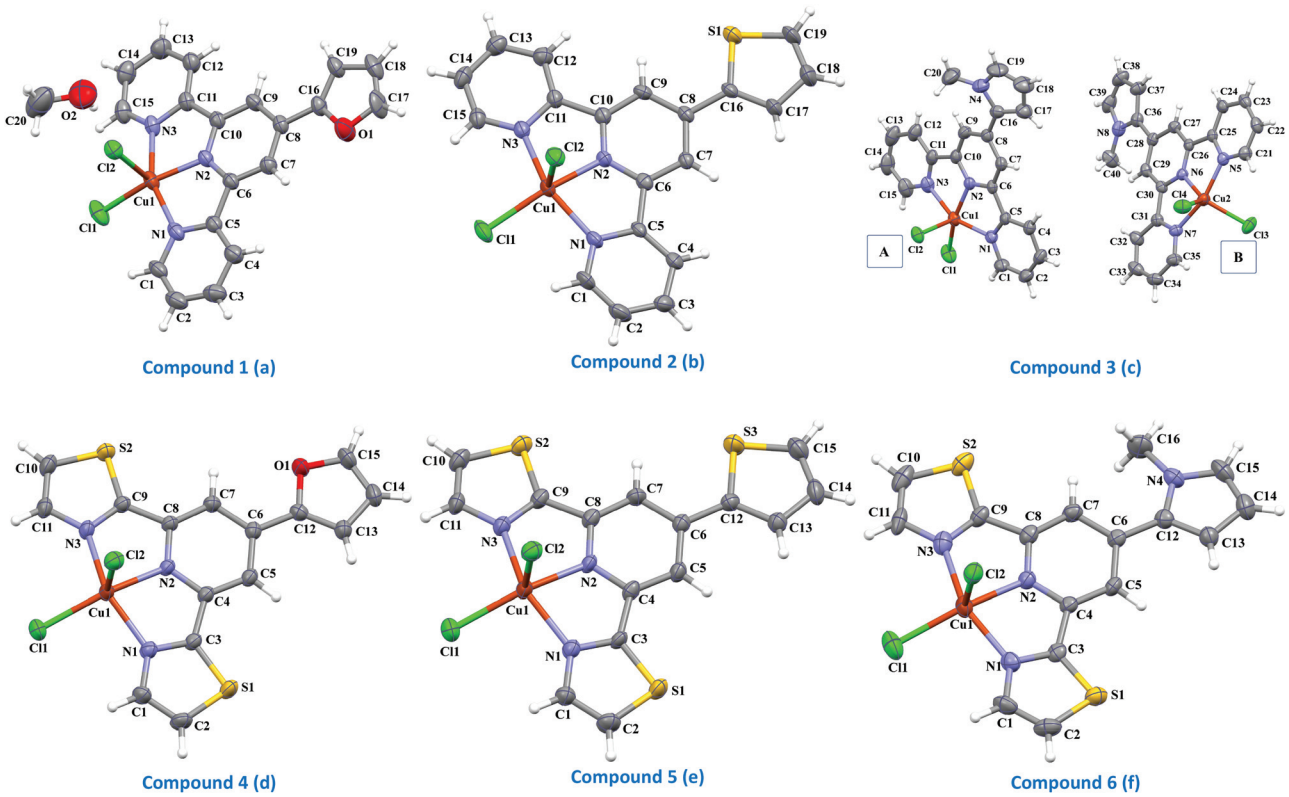

Fig. 2 Perspective views showing the asymmetric unit of **1** (a), **2** (b), **3** (c), **4** (d), **5** (e) and **6** (f) with the atom numbering. Displacement ellipsoids are drawn at the 50% probability level.

lated using the SHAPE program[15] based on the Continuous Shape Measures (CShM) concept.[16]

$$S_Q(P) = \min\left[\frac{\sum_{i=1}^{n}|\vec{q}_i - \vec{p}_i|^2}{\sum_{i=1}^{n}|\vec{q}_i - \vec{q}_0|^2}\right] \times 100$$

As seen in Table 1, the calculated values of S_Q(TBY) and S_Q(SPY) confirm that the coordination polyhedron of the Cu(1) ion is a square-pyramid, while the geometry around the Cu(2) center seems to be much closer to a trigonal bipyramid. In the other complexes examined herein, the metal center is in a square pyramid environment. It is noteworthy that the trigonal–bipyramidal geometry in the five-coordinate Cu(II) complexes incorporating 2,2′:6′,2″-terpyridines of general formula [$CuCl_2$(R-terpy)] is rather unusual. These compounds definitely prefer a square pyramidal geometry. CSD (Cambridge Structural Database, Version 5.37)[17] searches revealed only three complexes [$CuCl_2$(R-terpy)] which show a geometry closer

Table 1 Distortion of the coordination sphere of ions from ideal five-vertex polyhedra (square-pyramid (SPY) and trigonal bipyramid (TBY)) expressed as the angular structural index parameter τ[14] and calculated using the SHAPE program[15]

Compound	τ	S_Q(TBY)	S_Q(SPY)
1	0.132	6.296	1.626
2	0.072	5.697	1.712
3	0.077 (for Cu(1))	5.692 (for Cu(1))	1.611 (for Cu(1))
	0.457 (for Cu(2))	2.488 (for Cu(2))	3.940 (for Cu(2))
4	0.080	5.866	1.465
5	0.121	5.620	1.493
6	0.059	5.928	1.886

S_Q(TBY) – distortion of the coordination sphere of the Cu ion from ideal trigonal bipyramid. S_Q(SPY) – distortion of the coordination sphere of the Cu ion from ideal square pyramid.

to a trigonal bipyramid, while 16 structures can be described as a distorted square-pyramid (see Table S1†). The occurrence of a trigonal bipyramidal geometry in the case of **3** seems to be attributed to the presence of the bulky methyl substituent.

Typically for the square-pyramidal configuration, due to Jahn–Teller distortion,[18] the Cu–Cl apical bond in **1–6** is much longer than the Cu–Cl basal bond. The significant elongation of the Cu(1)–Cl(2) bond in **1** compared to the other complexes may be attributed to the formation of the hydrogen bond O(2)–H(2A)···Cl(2) [D···A distance = 3.195(3) Å and D–H···A angle = 170.10°] between the uncoordinated methanol molecules and [$CuCl_2$(R^1-terpy)]. As can be expected, a smaller difference between the apical and equatorial Cu–Cl bond lengths was observed for molecule **B** of **3**.

In all the complexes, the 2,2′:6′,2″-terpyridine and 2,6-di(thiazol-2-yl)pyridine skeletons are approximately planar. The maximum value of the dihedral angle between the mean planes of the terminal aromatic rings is 11.7° in complex **2**. The twisting of the R-substituent plane relative to the central pyridine ring assumes values from 4.0° (in **4**) to 19.10° (in the **A** molecule of **3**) (Table S3†). The two outer nitrogen atoms N(1) and N(2) form longer Cu–N bonds (**1**: 2.042(2) Å and 2.045(2) Å; **2**: 2.036(4) Å and 2.050(4) Å; **3A**: 2.043(2) Å and 2.051(2) Å; **3B**: 2.017(2) Å and 2.023(2) Å; **4**: 2.036(2) Å and 2.046(2) Å; **5**: 2.046(3) Å and 2.047(3) Å; **6**: 2.027(4) Å and 2.048(4) Å) than the central nitrogen atom (**1**: 1.941(2) Å; **2**: 1.939(3) Å; **3A**: 1.950(2) Å; **3B**: 1.955(2) Å; **4**: 1.976(2) Å; **5**: 1.977(2) Å; **6**: 1.979(4) Å). The same geometry and pattern of bond distances have been observed in most terpy complexes with copper(II) (Table S1†) or other divalent transition-metal ions.[13]

The crystal packing analysis (Mercury 2.4 program)[19] revealed that the dominant driving forces towards self-aggregation of molecules [$CuCl_2$(R^n-terpy)] and [$CuCl_2$(R^n-dtpy)] in the structures of **1–6** are weak hydrogen bonds C–H···Cl, (Table S4†) as well as π···π (Table S5†) and π···Cl (Table S6†) interactions. The R^1-terpy domains in **1** and R^n-dtpy moieties in **4** and **5** form layers, while molecules of **2**, **3** and **6** are packed into columns (Fig. 3 and Fig. S1†).

Cytotoxic potential

The *in vitro* antiproliferative activities of complexes **1–6** were analysed in four human tumour cell lines, HCT116, A2780, A549 and MCF7, by the application of the MTS colorimetric assay. This methodology relies on the reduction of MTS into a brownish formazan product by the mitochondrial dehydrogenases in metabolically active, viable cells.[20a,b] A decrease of the cell viability in a dose-dependent manner was observed for the four tumour cell lines after 48 h exposure to complexes **1–6** (Fig. 4).

In Table 2 the IC_{50} values for complexes **1–6** in tumour and normal cell lines are presented (at 48 h). The selectivity index was calculated for A2780 towards fibroblasts. As expected, the selectivity index is very high for complex **1**, indicating that

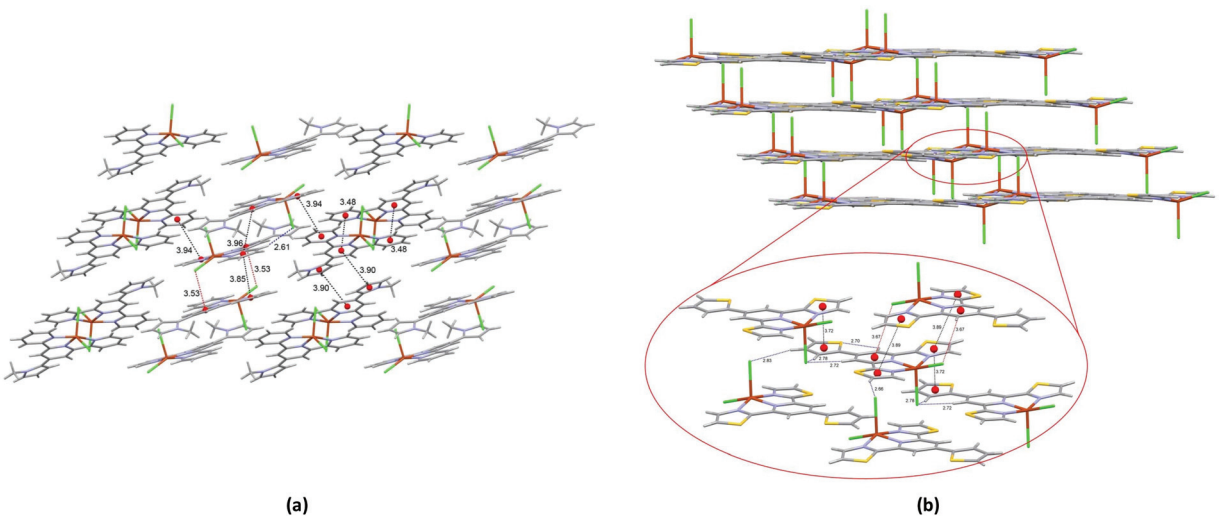

Fig. 3 View of the supramolecular packing of **3** (a) and **5** (b) arising from hydrogen bonds and weak π···π and π···Cl type interactions. For all structures of **1–6** see Fig. S1 of the ESI.†

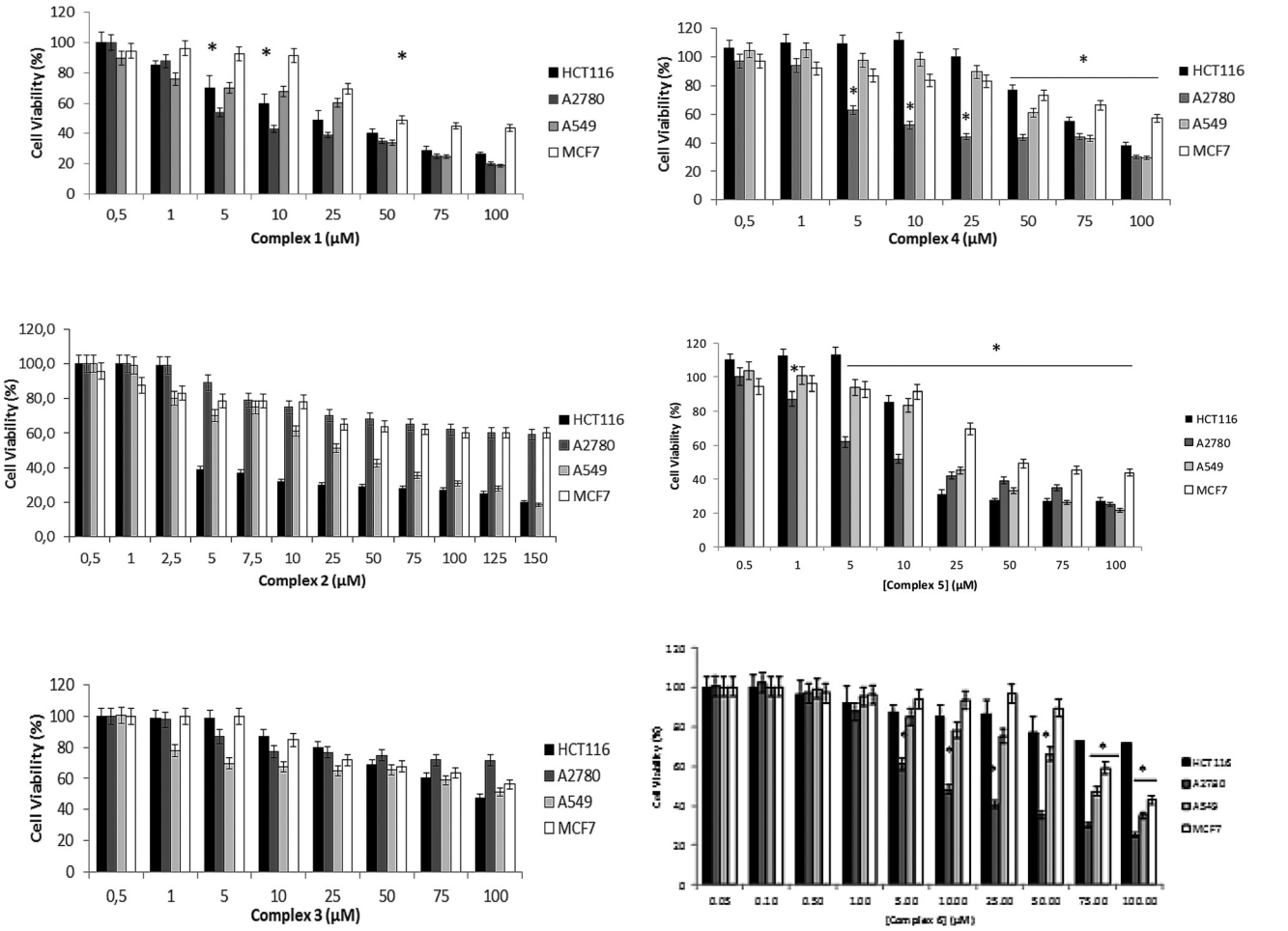

Fig. 4 Cytotoxicity of compounds **1–6** (a–f) in HCT116, A2780, A549 and MCF7 cell lines. HCT116 (black bars), A2780 (dark grey), A549 (light grey) and MCF7 (white bars) cells were treated with increasing concentrations of the complex for 48 h and cell viability was determined by the MTS assay. The data were normalized against the control treated with 0.1% (v/v) DMSO. The results shown are expressed as the mean ± SEM from three independent assays. The asterisk (*) in the figure means that the results are statistically significant with a $p < 0.05$ (as compared to the control for each cell line).

Table 2 The relative IC_{50} values for complexes **1–6** in tumour and normal cell lines (at 48 h)

	Relative IC_{50} (μM)					
Cell line	Complex **1**	Complex **2**	Complex **3**	Complex **4**	Complex **5**	Complex **6**
HCT116	17.3 ± 0.3	2.1 ± 0.1	>100	81.7 ± 0.3	20.5 ± 0.4	>100
A2780	2.9 ± 0.1	>100	>100	5.9 ± 0.1	4.6 ± 0.1	2.6 ± 0.1
A549	20.5 ± 0.2	4.2 ± 0.2	>100	64.3 ± 0.3	22.6 ± 0.3	70.1 ± 0.4
MCF7	43 ± 0.3	>100	>100	>100	62.3 ± 0.5	89 ± 0.5
Fibroblasts	59.5 ± 0.5	>100	>100	>100	23.4 ± 0.2	>100
Selectivity index	20.5	—	—	—	5	—

complex **1** is 20 times more selective for A2780 compared with normal human fibroblasts.

It is noteworthy that 2,6-di(thiazol-2-yl)pyridine derivatives (R^n-dtpy) (complexes **4**, **5** and **6**) demonstrate high specificity towards ovarian carcinoma cells (A2780), particularly with the R^3-substituent (Scheme 1, Table 2 and Fig. 4d–f) with moderate to low cytotoxicity for the other three cell lines (HCT116, A549 and MCF7). Interestingly, compared with the 2,2′:6′,2″-terpyridine (4′-R^n-terpy) complexes only complex **1** with the R^1-substituent demonstrates the same high specificity towards ovarian carcinoma cells (Scheme 1, Table 2 and Fig. 4a). This indicates that most of its cytotoxic effect in the ovarian carcinoma cell line can be correlated with the presence of the R^1-substituent in complex **1**. Indeed, complexes **2** and **3** (with R^2-

and R^3-substituents, respectively) do not show any antiproliferative activity in the ovarian carcinoma (A2780) cell line (Scheme 1, Table 2 and Fig. 4b–c). The IC_{50} values (Table 2) demonstrate that complex **2** (with the R^2-substituent) seems to be highly specific towards colorectal carcinoma (HCT116) and lung adenocarcinoma (A549) cells (Table 2 and Fig. 4b). Of relevance is the fact that the trigonal bipyramidal geometry in the case of **3** (attributed to the presence of the bulky methyl substituent) instead of the more common square pyramidal one (other Cu(II) complexes) does not show any cytotoxic activity in tumour cell lines (Fig. 4c and Table 2).

Except for complex **5** that shows moderate activity towards normal human fibroblasts, the other complexes **1–4** and **6** do not exhibit an antiproliferative activity against normal human

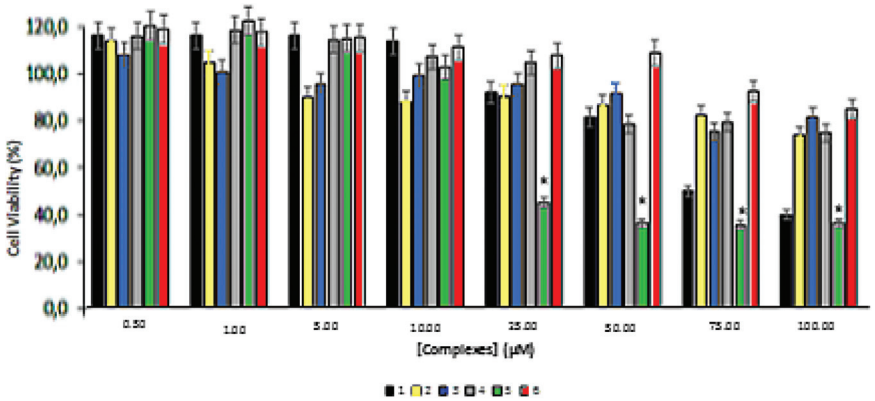

Fig. 5 Cytotoxicity of complexes **1–6** in normal human fibroblasts. Fibroblasts were treated with increasing concentrations of complexes **1** (black), **2** (very dark grey), **3** (dark grey), **4** (grey), **5** (light grey) and **6** (white) for 48 h and cell viability was determined by the MTS assay. The data were normalized against the control treated only with 0.1% (v/v) DMSO. The results shown are expressed as the mean ± SEM from three independent assays. The asterisk (*) in the figure means that the results are statistically significant with a $p < 0.05$ (as compared to the control for each complex).

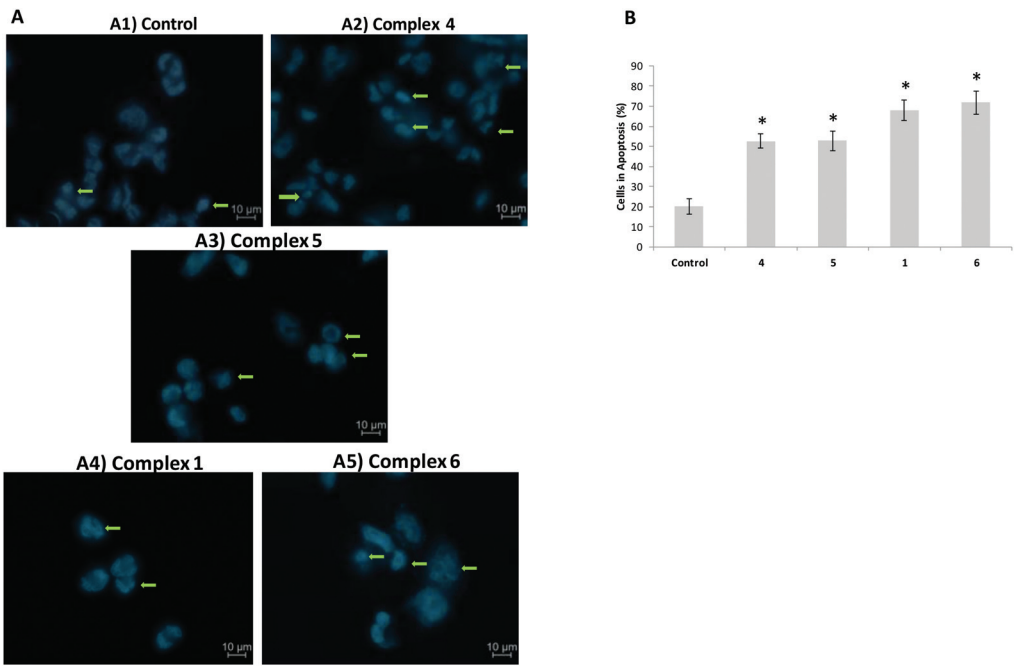

Fig. 6 Apoptotic morphological changes in A2780 cells exposed to complexes **1**, **4**, **5** and **6**. A. Hoechst staining of the A2780 cell line for the visualization of apoptotic nuclei (excitation and fluorescence emission spectra at 352/461 nm, respectively). Cells were grown in DMEM culture medium supplemented with 10% foetal bovine serum in the presence of (A1) 0.1% DMSO (control), (A2) the IC_{50} of complex **4**, (A3) the IC_{50} of complex **5**, (A4) the IC_{50} of complex **1**, and (A5) the IC_{50} of complex **6** for 48 h and stained with Hoechst 33258. Plates were photographed on an AXIO Scope (Carl Zeiss, Oberkochen, Germany). Typical morphological features of apoptosis like chromatin condensation and nuclear fragmentation are identified (green arrows). B. The value in % of apoptotic cells after exposure of A2780 cells to the control vehicle (DMSO) or complexes **4**, **5**, **1** and **6**. Three random microscopic fields per sample with *ca*. 50 nuclei were counted. *p-Value <0.05 relative to apoptosis in cells incubated with DMSO.

fibroblasts at the concentrations tested (IC_{50} higher than 50 μM) (see Fig. 5 and Table 2).

Cytoreductive surgery plus platinum based chemotherapy is the first line of treatment in ovarian cancer, but due to chemoresistance, this therapy has limited efficacy.[20c] In this regard, to compare the effect of our complexes with that of cisplatin on ovarian carcinoma cells we have studied under the same experimental conditions the effect of cisplatin on A2780 cell viability (ESI Fig. 6†). The relative IC_{50} observed for cisplatin is 3.4 ± 0.2 μM, which is similar to the IC_{50} observed for complexes **1**, **4**, **5** and **6** (Table 2). Indeed, compared to cisplatin, complexes **1** and **6** show a higher cytotoxicity towards the A2780 cell line, demonstrating their promising effect, which should be considered in further biological studies.

Apoptotic potential

The reduction of cell viability promoted by complexes **1–6** in A2780 cells (Fig. 4c) prompted us to evaluate the underlying mechanisms of cell death. A preliminary analysis was performed by staining using Hoechst 33258 dye owing to its high affinity for DNA allowing the detection of nuclear alterations like chromatin condensation and nuclear fragmentation, typical features of apoptotic cells.[21] Hoechst 33258 staining of A2780 cells after 48 h of exposure to the IC_{50} of each relevant complex allowed us to observe a reduction in the number of stained cells compared to control cells and the nuclear condensation and fragmentation characteristics of apoptosis (Fig. 6). Hoechst 33258 staining of HCT116 cells after 48 h of exposure to the IC_{50} of complex **2** is also shown in Fig. 6. As we can observe (Fig. 6 and 7) the induction of apoptosis totally agrees with the viability results presented before.

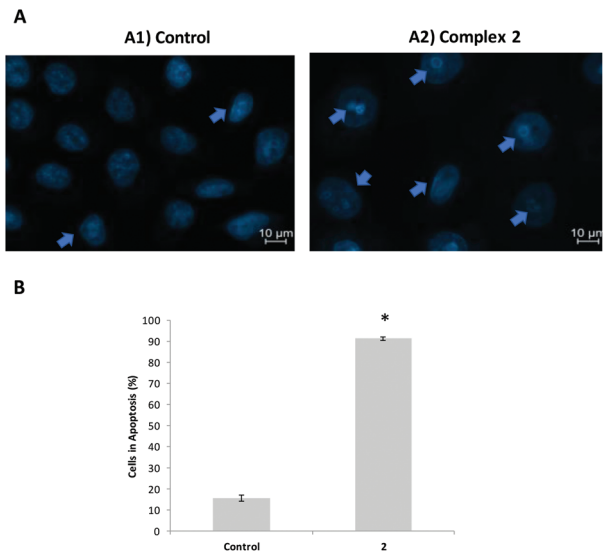

Fig. 7 Apoptotic morphological changes in HCT116 cells exposed to complex **2**. A. Hoechst staining of the HCT116 cell line for the visualization of apoptotic nuclei (excitation and fluorescence emission spectra at 352/461 nm, respectively). Cells were grown in DMEM culture medium supplemented with 10% foetal bovine serum in the presence of (A1) 0.1% DMSO (control) and (A2) the IC_{50} of complex **2** for 48 h and stained with Hoechst 33258. Plates were photographed on an AXIO Scope (Carl Zeiss, Oberkochen, Germany). Typical morphological features of apoptosis like chromatin condensation and nuclear fragmentation are identified (green arrows). B. The value in % of apoptotic cells after exposure of HCT116 cells to the control vehicle (DMSO) or complex **2**. Three random microscopic fields per sample with *ca.* 50 nuclei were counted. **p*-Value <0.05 relative to apoptosis in cells incubated with DMSO.

Catalytic oxidation of alkanes and alcohols with peroxides

Copper ions constitute the reaction centres of some alcohol- and alkane-oxidizing enzymes.[22] Copper complexes are known to catalyze the oxygenation of alkanes into alkyl hydroperoxides[23] and oxidize alcohols into the corresponding ketones (aldehydes).[9a,24] Molecular oxygen and various peroxides (H_2O_2, *tert*-butyl hydroperoxide, peroxyacetic acid, *meta*-chloroperoxybenzoic acid) were used as oxidants.

As has been mentioned above, the oxygenation of saturated hydrocarbons such as RH, as well as of some alkane derivatives with H_2O_2, usually gives rise to the formation of the corresponding alkyl hydroperoxides, ROOH, as the main primary products. We use a simple method developed earlier by one of us[25] to demonstrate the formation of alkyl hydroperoxide in this oxidation and to estimate its concentration in the course of the reaction. If an excess of solid PPh_3 is added to the sample of the reaction solution before the GC analysis, the alkyl hydroperoxide present is completely reduced to the corresponding alcohol. Comparing the measured by GC concentrations of the alcohol and ketone before and after reduction with PPh_3, we can estimate the real concentrations of the three products (alkyl hydroperoxide, ketone and alcohol) present in the reaction solution. In many experiments we determined the concentrations of isomers only after reduction with PPh_3.

Two examples of cyclohexane oxidation with H_2O_2 catalyzed by complexes **4** and [$CuCl_2$(terpy)] are shown in Fig. 8. The most active catalyst **4** gave, after 120 min, 0.105 M of cyclohexanol + cyclohexanone after reduction with PPh_3. This concen-

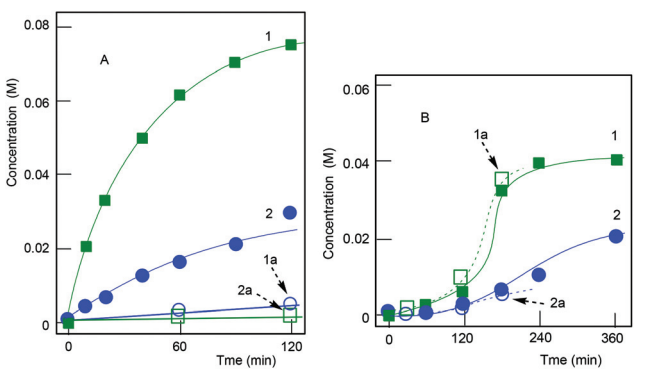

Fig. 8 Accumulation of cyclohexanol (curves 1) and cyclohexanone (curves 2) in the oxidation of cyclohexane (0.46 M) with H_2O_2 (2.0 M) catalyzed by compound **4** (Graph A) or [Cu(terpy)Cl_2] (Graph B), concentrations 5 × 10^{-4} M in acetonitrile solution at 60 °C. Curves 1a and 2a correspond to the experiments with the addition of HNO_3 (0.05 M).

tration corresponds to a yield of 23% and TON = 210. Fig. 9 shows that in the cyclohexane oxidation with H_2O_2 catalyzed by complex **2** the alcohol/ketone ratio is dramatically changed when a reducing agent is added. This ratio is different for PPh_3 and thiourea as reductants, which indicates the formation of alkyl hydroperoxides in this reaction.

It can be clearly seen in Fig. 8 and 9 that the oxidation occurs with auto-acceleration. This phenomenon testifies that in the beginning of the reaction the starting complex is rather slowly transformed into a catalytically active form. Table 3 compares the activities of the complexes after 120 min. The complexes exhibit different activities in cyclohexane oxidation.

In order to determine the nature of the alkane-oxidizing species, we measured the selectivity parameters in the oxidations of certain alkanes with H_2O_2 catalyzed by complex **4**. The selectivity parameter (1.0 : 6.0 : 5.6 : 4.7) is similar to the selectivity parameters determined previously for systems generating free hydroxyl radicals.[26] Catalyzed by **4**, hydrogen peroxide oxidation of *cis*-1,2-dimethylcyclohexane gave *tert*-alcohols with a 0.8 ratio of isomers with mutual *trans*- and *cis*-orientation of methyl groups. These data indicate that the oxidation proceeds with the participation of free hydroxyl radicals.[26] Oxidation of 1,2-dimethylcyclohexane with *m*-CPBA catalyzed by **4** in the presence of HNO_3 gave a product of a stereoselective reaction (*trans*/*cis* = 0.47). However, this parameter has been found to be *trans*/*cis* = 0.8 for the catalysis by **4** in the absence of HNO_3.

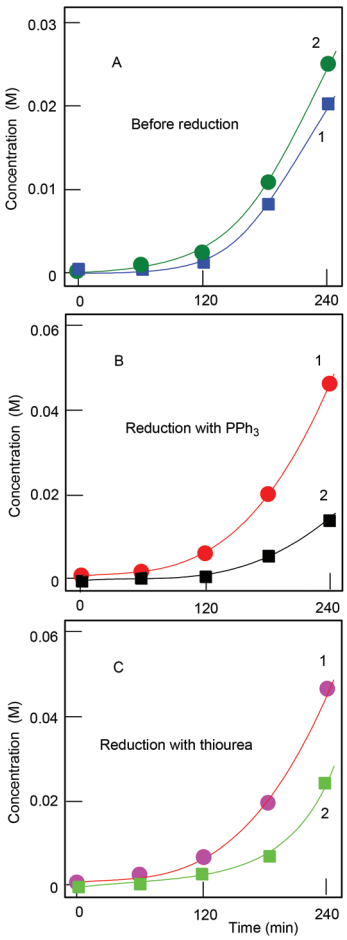

Fig. 9 Accumulation of cyclohexanol (curves 1) and cyclohexanone (curves 2) in the oxidation of cyclohexane (0.46 M) with H_2O_2 (1.5 M) catalyzed by compound **2** (concentrations 5×10^{-4} M) in acetonitrile solution at 60 °C. The samples of the reaction solution were not reduced (graph A), reduced with PPh_3 (graph B), or thiourea (graph C).

Table 3 Comparison of various copper-containing catalysts in cyclohexane oxidation with H_2O_2 [a]

Entry	Catalyst	Yield of oxygenates (M)	Total yield (%)	TON
1	**4**	0.105	23	210
2	[Cu(terpy)Cl_2]	0.059	13	118
3	**5**	0.057	12	114
4	**3**	0.044	9.6	88
5	**2**	0.040	8.7	80
6	**6**	0.023	5	46
7	**1**	0.008	2	16

[a] The yields of cyclohexanol and cyclohexanone were measured after 120 min heating at 60 °C and after reduction of the reaction samples with PPh_3.

We have also found that secondary alcohols can be oxidized into ketones with hydrogen peroxide or TBHP if the copper complexes prepared in this work are used as catalysts. Some results are presented in Table 4. It can be seen that the yield of the target ketones reached 98% and TON = 630.

$$PhCH(OH)CH_3 + \textit{tert}\text{-}BuOOH + O_2 \rightarrow PhC(=O)CH_3$$

Table 4 Alcohol oxidation with TBHP catalyzed by various copper-containing complexes[a]

Entry	Alcohol	Catalyst	*T* (°C)	Time (min)	Yield (%)	TON
1	PhCH(OH)CH_3	**4**	50	15	10	
2	PhCH(OH)CH_3	**4**	50	120	39	
3	PhCH(OH)CH_3	**4**	50	300	51	
4	PhCH(OH)CH_3	**4**	50	480	80	520
5	PhCH(OH)CH_3	**4**	60	90	56	
6	PhCH(OH)CH_3	**4**	60	180	82	
7	PhCH(OH)CH_3	**4**	60	300	94	620
8	PhCH(OH)CH_3	**4**	60	90	56	
9	PhCH(OH)CH_3	**4**	60	180	82	
10	PhCH(OH)CH_3	**4**	60	300	98	630
11	Cyclohexanol	**3**	60	60	39	
12	Cyclohexanol	**3**	60	180	39	
13	Cyclohexanol	**3**	60	300	40	344
14	Cyclohexanol	**3**	60	480	43	
15	Cyclohexanol	**2**	60	60	39	
16	Cyclohexanol	**2**	60	180	49	
17	Cyclohexanol	**2**	60	300	56	
18	Cyclohexanol	**2**	60	480	65	520
19	Cyclohexanol	**4**	60	60	48	
20	Cyclohexanol	**4**	60	180	60	
21	Cyclohexanol	**4**	60	330	71	580

[a] The yields of cyclohexanol and cyclohexanone were measured after 120 min heating at 60 °C and after reduction of the reaction samples with PPh_3.

Conclusions

Six new copper(II) complexes incorporating 2,2′:6′,2″-terpyridine and 2,6-di(thiazol-2-yl)pyridine-based ligands have been synthesized and characterized. Two applied studies of these complexes were conducted. Thus, the antiproliferative potential of the copper(II) complexes of 2,2′:6′,2″-terpyridine (R^n-terpy) and 2,6-di(thiazol-2-yl)pyridine (R^n-dtpy) derivatives was examined towards human colorectal (HCT116) and ovarian (A2780) carcinoma as well as towards lung (A549) and breast adenocarcinoma (MCF7) cell lines. Complex **1** and complex **6** were found to have the highest antiproliferative effect on A2780 ovarian carcinoma cells, particularly when compared with complexes **2** and **3** with no antiproliferative effect. The order of cytotoxicity in this cell line is **6** > **1** > **5** > **4** > **2** ≈ **3**. Complex **2** seems to be much more specific towards colorectal carcinoma HCT116 and lung adenocarcinoma A549 cells. The viability loss induced by the complexes was in agreement with Hoechst 33258 staining and typical morphological apoptotic characteristics like chromatin condensation and nuclear fragmentation.

The specificity, towards different types of cell lines, of these 2,2′:6′,2″-terpyridine (R^n-terpy) and 2,6-di(thiazol-2-yl)pyridine (R^n-dtpy) derivatives and their low cytotoxic activity towards healthy cells are of particular interest and are a positive feature for further developments. These complexes exhibited different catalytic activities in the oxidation of alkanes and alcohols with peroxides.

Experimental

Materials

All the solvents used in the synthesis were of reagent grade and were used as received. The salt $CuCl_2{\cdot}2H_2O$ used in the synthesis was commercially available and was used without further purification. 4′-Functionalized 2,2′:6′,2″-terpyridine and 2,6-di(thiazol-2-yl)pyridine derivatives were prepared according to a literature method.[4b,10c,12,27]

Instrumentation

The IR spectra were recorded on a Nicolet iS5 spectrophotometer in the spectral range 4000–400 cm^{-1} with samples in the form of KBr pellets. The electronic spectra were obtained using a Nicolet Evolution 220 in the ranges of 210–1000 nm in methanol (see the ESI†) and 190–1100 nm in solid state samples. Powder X-ray diffraction (PXRD) measurements were performed on a PANalytical Empyrean X-ray diffractometer using Cu-Kα radiation (λ = 1.5418 Å), in which the X-ray tube was operated at 40 kV and 30 mA in the range of 0 to 50°.

The X-ray diffraction data were collected on an Oxford Diffraction four-circle diffractometer Gemini A Ultra equipped with an Atlas CCD detector using graphite monochromated Mo Kα radiation (λ = 0.71073 Å) at room temperature. Details of crystal data and refinement are given in Table 5. Lorentz, polarization and empirical absorption corrections using spherical harmonics implemented in the SCALE3 ABSPACK scaling algorithm[28] were applied. The structures were solved by the Patterson method using SHELXS97 and refined by full-matrix least-squares on F^2 using SHELXL97.[29] All the non-hydrogen atoms were refined anisotropically, and hydrogen atoms were placed at calculated positions refined using idealized geometries (riding model) and assigned fixed isotropic displacement parameters, d(C–H) = 0.93 Å, U_{iso}(H) = 1.2U_{eq}(C).

Synthesis of the complexes

General synthesis route for [$CuCl_2(R^n$-terpy)] (1–3), [$CuCl_2(R^n$-dtpy)] (4–6) and [$CuCl_2$(terpy)]. The salt $CuCl_2{\cdot}2H_2O$ (0.17 g, 1 mmol) dissolved in methanol (10 ml) was added dropwise to hot methanolic solutions of R^n-terpy, R^n-dtpy or terpy (1 mmol). The resulting solution was stirred at room temperature for 2 h and after a few days green crystalline solids were obtained. Crystals suitable for X-ray investigation were obtained by recrystallization from methanol or acetonitrile.

[$CuCl_2(R^1$-terpy)] (1). Yield 64%. HRMS (ESI): calcd for $C_{19}H_{13}ClCuN_3O^+$ 397.0043 found 397.0055. IR (KBr, cm^{-1}): 1615(s), 1583(m) 1560(m), 1475(s), 1435(m), 1385(w), 1304(m), 1255(m), 1235(w), 1157(w), 1027(s), 1019(s), 883(m), 793(s), 751(m), 741(m), 729(m), 687(m), 655(m), 645(w), 586(w). UV-Vis (MeOH, λ_{max}, nm (ε, dm^3 mol^{-1} cm^{-1})): 222(35 700), 261(23 700), 289(21 300), 347(31 000) and 701(131). UV-Vis (solid, nm): 302, 319, 366 and 720.

[$CuCl_2(R^2$-terpy)] (2). Yield 79%. HRMS (ESI): calcd for $C_{19}H_{13}ClCuN_3S^+$ 412.9815 found 412.9821. IR (KBr, cm^{-1}): 1607(s), 1569(m), 1559(s), 1528(m), 1474(s), 1429(s), 1377(w), 1252(m), 1165(m), 1053(m), 1033(m), 1018(m), 892(w), 859(m), 793(s), 778(m), 751(m), 729(m), 702(s), 655(w), 627(m), 560(w). UV-Vis (MeOH, λ_{max}, nm (ε, dm^3 mol^{-1} cm^{-1})): 221(31 300), 266(20 700), 287(21 300), 347(25 300) and 701(134). UV-Vis (solid, nm): 225, 285, 322, and 727.

[$CuCl_2(R^3$-terpy)] (3). Yield 71%. HRMS (ESI): calcd for $C_{20}H_{16}ClCuN_4^+$ 410.0359 found 410.0359. IR (KBr, cm^{-1}): 1610.78(s), 1568(m), 1555(m), 1534(w), 1475(s), 1431(s), 1400(m), 1302(m), 1274(m), 1255(w), 1245(m), 1156(m), 1077(m), 1066.29(w), 1030(m), 1019(m), 998(m), 792(s), 735(w), 719(m), 676(m), 646(w), 600(w). UV-Vis (MeOH, λ_{max}, nm (ε, dm^3 mol^{-1} cm^{-1})): 220(36 900), 266(23 900), 276(21 021), 320(16 600), 389(18 900) and 701(115). UV-Vis (solid, nm): 231, 273, 317, 366 and 735.

[$CuCl_2(R^1$-dtpy)] (4). Yield 70%. HRMS (ESI): calcd for $C_{15}H_9ClCuN_3OS_2^+$ 408.9172 found 408.9171. IR (KBr, cm^{-1}): 1610(s), 1578(m), 1550(m), 1489(s), 1455(s), 1437(m), 1386(m), 1355(w), 1267(w), 1240(m), 1193(s), 1148(w), 1101(w), 1063(m), 1037(m), 1020(s), 919(m), 881(m), 856(m), 786(s), 762(s), 742(s), 637(m), 596(m), 577(w). UV-Vis (MeOH, λ_{max}, nm (ε, dm^3 mol^{-1} cm^{-1})): 276(19 700), 308(28 100), 352(31 000) and 741(128). UV-Vis (solid, nm): 231, 297, 379 and 787.

[$CuCl_2(R^2$-dtpy)] (5). Yield 82%. HRMS (ESI): calcd for $C_{15}H_9ClCuN_3S_3^+$ 424.8943 found 424.8942. IR (KBr, cm^{-1}): 1611(s), 1551(m), 1526, 1496(s), 1483(m), 1452(m), 1419(m), 1404(m), 1364(m), 1266(m), 1245(m), 1206(s), 1196(s), 1147(w), 1099(m), 1021(w), 915(m), 848(m), 787(s), 773(w), 757(w),

Table 5 Crystal data and structure refinement of copper(II) complexes

	(1)	(2)	(3)	(4)	(5)	(6)
Empirical formula	$C_{20}H_{17}Cl_2CuN_3O_2$	$C_{19}H_{13}Cl_2CuN_3S$	$C_{20}H_{16}Cl_2Cu\ N_4$	$C_{15}H_9Cl_2CuN_3OS_2$	$C_{15}H_9Cl_2CuN_3S_3$	$C_{16}H_{12}Cl_2CuN_4S_2$
Formula weight	465.80	449.82	446.81	445.81	461.87	458.86
Temperature [K]	295.0(2)	295.0(2)	295.0(2)	295.0(2)	295.0(2)	295.0(2)
Wavelength [Å]	0.71073	0.71073	0.71073	0.71073	0.71073	0.71073
Crystal system	Triclinic	Monoclinic	Triclinic	Triclinic	Triclinic	Orthorhombic
Space group	$P\bar{1}$	$P2_1/c$	$P\bar{1}$	$P\bar{1}$	$P\bar{1}$	$Pna2_1$
Unit cell dimensions [Å, °]	a = 7.9205(5) b = 10.6701(6) c = 12.6536(8) α = 106.766(5) β = 97.488(5) γ = 102.659(5)	a = 7.8185(4) b = 11.0960(7) c = 20.4983(12) β = 95.626(5)	a = 9.3952(3) b = 12.8556(4) c = 16.9843(6) α = 72.580(3) β = 81.358(3) γ = 73.642(3)	a = 7.8472(4) b = 10.3540(6) c = 11.2776(7) α = 116.387(6) β = 95.253(5) γ = 90.856(4)	a = 7.8330(4) b = 10.9863(8) c = 11.2152(8) α = 118.351(7) β = 92.578(5) γ = 91.767(6)	a = 21.3169(8) b = 10.9680(5) c = 7.5747(4)
Volume [Å^3]	977.37(11)	1769.74(18)	1873.19(11)	815.80(9)	847.01(11)	1770.99(14)
Z	2	4	4	2	2	4
Density (calculated) [Mg m^{-3}]	1.583	1.688	1.584	1.815	1.811	1.721
Absorption coefficient [mm^{-1}]	1.412	1.662	1.464	1.929	1.976	1.778
F(000)	474	908	908	446	462	924
Crystal size [mm]	0.28 × 0.07 × 0.05	0.22 × 0.05 × 0.02	0.16 × 0.14 × 0.09	0.36 × 0.06 × 0.03	0.50 × 0.05 × 0.03	0.55 × 0.27 × 0.07
θ range for data collection [°]	3.32 to 25.05	3.43 to 25.05	3.30 to 25.05	3.37 to 25.05	3.36 to 25.04	3.30 to 25.05
Index ranges	$-9 \le h \le 9$ $-11 \le k \le 12$ $-14 \le l \le 15$	$-9 \le h \le 9$ $-13 \le k \le 11$ $-24 \le l \le 23$	$-11 \le h \le 10$ $-15 \le k \le 14$ $-20 \le l \le 20$	$-9 \le h \le 9$ $-12 \le k \le 11$ $-13 \le l \le 13$	$-9 \le h \le 9$ $-13 \le k \le 12$ $-13 \le l \le 12$	$-25 \le h \le 25$ $-12 \le k \le 13$ $-9 \le l \le 7$
Reflections collected	8026	7539	15 611	6826	6680	7628
Independent reflections	3468 (R_{int} = 0.0351)	3126 (R_{int} = 0.0508)	6636 (R_{int} = 0.0338)	2888 (R_{int} = 0.0356)	2993 (R_{int} = 0.0335)	2958 (R_{int} = 0.0340)
Completeness to 2θ = 50° [%]	99.8	99.8	99.8	99.7	99.8	99.8
Max. and min. transmission	1.000 and 0.747	1.000 and 0.776	1.000 and 0.805	1.000 and 0.134	1.000 and 0.752	1.000 and 0.393
Data/restraints/parameters	3468/0/255	3126/0/235	6636/0/489	2888/0/217	2993/0/217	2958/0/227
Goodness-of-fit on F^2	1.012	1.040	1.034	1.039	1.025	1.038
Final R indices [$I > 2\sigma(I)$]	R_1 = 0.0369 wR_2 = 0.0803	R_1 = 0.0538 wR_2 = 0.1323	R_1 = 0.0354 wR_2 = 0.0838	R_1 = 0.0333 wR_2 = 0.0680	R_1 = 0.0359 wR_2 = 0.0812	R_1 = 0.0316 wR_2 = 0.0683
R indices (all data)	R_1 = 0.0544 wR_2 = 0.0863	R_1 = 0.0715 wR_2 = 0.1415	R_1 = 0.0515 wR_2 = 0.0900	R_1 = 0.0513 wR_2 = 0.0705	R_1 = 0.0513 wR_2 = 0.0878	R_1 = 0.0382 wR_2 = 0.0715
Largest diff. peak and hole [e Å^{-3}]	0.271 and −0.297	1.038 and −0.583	0.383 and −0.274	0.319 and −0.377	0.475 and −0.518	0.247 and −0.352
CCDC number	1540061	1540064	1540062	1540063	1540065	1540066

740(s), 625(w), 614(m), 564(w). UV-Vis (MeOH, λ_{max}, nm (ε, dm^3 mol^{-1} cm^{-1})): 304(20 800), 352(18 400) and 736(116). UV-Vis (solid, nm): 295 and 802.

[CuCl$_2$(R^3-dtpy)] (6). Yield 45%. HRMS (ESI): calcd for $C_{16}H_{12}ClCuN_4S_2^+$ 421.9488 found 421.9488. IR (KBr, cm^{-1}): 1603(s), 1599(s), 1544(m), 1536(m), 1498(m), 1481(s), 1442(m), 1417(m), 1395(s), 1351(m), 1337(m), 1292(m), 1242(m), 1206(m), 1194(m), 1074.20(s), 1020(m), 999(m), 821(w), 797(m), 787(s), 771(m), 749(s), 677(w), 638(w), 588(w). UV-Vis (MeOH, λ_{max}, nm (ε, dm^3 mol^{-1} cm^{-1})): 274(23 300), 300(22 100), 338(20 700), 391(15 700) and 741(110). UV-Vis (solid, nm): 356 and 763.

Cell culture

Human colorectal (HCT116) and ovarian carcinoma (A2780) cell lines and the lung adenocarcinoma (A549) cell line were grown in Dulbecco's modified Eagle's medium (DMEM) (Invitrogen Corp., Grand Island, NY, USA) supplemented with 10% fetal bovine serum and 1% antibiotic/antimycotic solution (Invitrogen Corp.) and maintained at 37 °C under a humidified atmosphere of 5% (v/v) CO_2.[30] MCF7 cells derived from pleural effusion of breast adenocarcinoma from a female patient were grown under similar conditions, supplemented with 1% MEM non-essential amino acids (Invitrogen Corp.).[30] Normal human fibroblasts were grown under the same conditions as the MCF7 cell line[31] All cell lines were purchased from ATCC (http://www.atcc.org) with the exception of A2780 that was purchased from Sigma-Aldrich (http://www.sigmaaldrich.com).

Compound exposure for dose–response curves

Cells were plated at 5000 cells per well in 96-well plates. The medium was removed 24 h after plating and was replaced with a fresh medium containing: 0.1–200 μM of complexes **1–6** or 0.1% (v/v) DMSO (vehicle control). All the above solutions were

prepared from concentrated stock solutions (in DMSO) of complexes **1–6**.

Viability assays

After 48 h of cell incubation in the presence or absence of complexes **1–6**, cell viability was evaluated using a CellTiter 96® AQueous Non-Radioactive Cell Proliferation Assay (Promega, Madison, WI, USA), using 3-(4,5-dimethylthiazol-2-yl)-5-(3-carboxymethoxyphenyl)-2-(4-sulfophenyl)-2*H*-tetrazolium, inner salt (MTS) as previously described.[20] In brief, this is a homogeneous, colorimetric method for determining the number of viable cells in proliferation, cytotoxicity or chemosensitivity assays. The CellTiter 96® AQueous Assay is composed of solutions of MTS and an electron coupling reagent (phenazinemethosulfate, PMS). MTS is bioreduced by cells into a formazan product that is soluble in a tissue culture medium. The absorbance of the formazan product at 490 nm can be measured directly from 96-well assay plates without additional processing. The conversion of MTS into the aqueous soluble formazan product is accomplished by using dehydrogenase enzymes found in metabolically active cells. The quantity of formazan product was measured on a Bio-Rad microplate reader, model 680 (Bio-Rad, Hercules, CA, USA), at 490 nm, as absorbance is directly proportional to the number of viable cells in culture.

Assessment of apoptosis through Hoechst 33258 staining

A2780 cells grown as described above were plated at 7500 cells per ml and incubated for 48 h in a culture medium containing each complex or 0.1% (v/v) DMSO (vehicle control). Hoechst staining was used to detect apoptotic nuclei as previously described.[30] Briefly, the medium was removed, cells were washed with phosphate-buffered saline 1× (PBS) (Invitrogen), fixed with 4% (v/v) paraformaldehyde in PBS 1× (10 min in the dark) and incubated with Hoechst 33258 dye (Sigma, Missouri, USA; 5 μg ml^{-1} in PBS 1×) for another 10 min. After being washed with PBS 1×, cells were mounted into 20 μL of a PBS : glycerol (3 : 1; v/v) solution. Fluorescent nuclei were sorted out according to the chromatin condensation degree and characteristics. Normal nuclei showed non-condensed chromatin uniformly distributed over the entire nucleus. Apoptotic nuclei showed condensate or fragmented chromatin. Some cells formed apoptotic bodies. Plates were photographed on an AXIO Scope (Carl Zeiss, Oberkochen, Germany), and three random microscopic fields per sample with *ca*. 50 nuclei were counted. The mean values are expressed as a percentage of apoptotic nuclei.[30]

Statistical analysis

All data are expressed as the mean ± SEM from at least three independent experiments. Statistical significance was evaluated using a Student's *t*-test; $p < 0.05$ was considered statistically significant.

Catalytic oxidation of alkanes and alcohols

Typically, reactions were carried out in air in thermostated Pyrex cylindrical vessels with vigorous stirring; the total volume of the reaction solution was 5 mL. Catalysts were introduced into the reaction solution in acetonitrile containing a substrate and an oxidizing reagent. (**CAUTION**: the combination of air or molecular oxygen and peroxides with organic compounds at elevated temperatures may be explosive!)

Samples of the reaction mixture obtained in the oxidation of alkanes and linear alcohols were taken after certain time intervals, and the concentrations of products were measured using the GC method In the oxidations of alkanes and benzene, the chromatograph-3700 (fused silica capillary column FFAP/OV-101 20/80 w/w, 30 m × 0.2 mm × 0.3 μm; helium as a carrier gas) was used. Attribution of peaks was made by comparison with chromatograms of authentic samples. Blank experiments with cyclohexane showed that in the absence of a catalyst, no products were formed. The samples obtained in the alkane oxidation were typically analyzed twice (before and after their treatment with PPh_3 or thiourea). This method (an excess of solid triphenylphosphine or thiourea is added to the samples 10–15 min before the GC) was proposed by one of us earlier[25] and allows us to detect alkyl hydroperoxides and measure also the real concentrations of all three products (alkyl hydroperoxide, alcohol and aldehyde or ketone) present in the reaction solution. In order to precisely determine the concentrations of isomeric alkanols, samples of the reaction solutions after addition of nitromethane were analyzed only after reduction with PPh_3.

The ^{1}H NMR method was used for the quantification of the acetophenone (Bruker AMX-400 instrument, 400 MHz) formed in the oxidation of 1-phenylethanol. Added to the sample acetone-d_6 was used as a component of the solvent (in addition to acetonitrile); 1,4-dinitrobenzene was used as a standard. The detection and quantification of the obtained products of the catalytic reactions were performed by measuring the areas of the peaks corresponding to the methyl group from acetophenone (2.6 ppm).

Conflict of interest

The authors declare no financial interest.

Acknowledgements

This work was supported by the National Science Centre of Poland (Grant No. DEC-2015/17/N/ST5/03892), the Russian Foundation for Basic Research (Grant No. 16-03-00254) and the Unidade de Ciências Biomoleculares Aplicadas-UCIBIO, which is financed by national funds from the FCT/MEC (UID/Multi/04378/2013) and co-financed by the ERDF under the PT2020 Partnership Agreement (POCI-01-0145-FEDER-007728).

References

1 (*a*) L. Hou, D. Li, W.-J. Shi, Y.-G. Yin and S. W. Ng, *Inorg. Chem.*, 2005, **44**, 7825–7832; (*b*) U. S. Schubert, H. Hofmeier and G. R. Newkome, in *Modern Terpyridine Chemistry*, Wiley-VCH Verlag GmbH & Co. KGaA, 2006, pp. 37–68; (*c*) Z. Naseri, A. N. Kharat, A. Banavand, A. Bakhoda and S. Foroutannejad, *Polyhedron*, 2012, **33**, 396–403; (*d*) Y. Guo, X.-L. Yang, R.-J. Wei, L.-S. Zheng and J. Tao, *Inorg. Chem.*, 2015, **54**, 7670–7672; (*e*) T. Ezhilarasu, A. Sathiyaseelan, P. T. Kalaichelvan and S. Balasubramanian, *J. Mol. Struct.*, 2017, **1134**, 265–277.

2 (*a*) H. Yamazaki, T. Ueno, K. Aiso, M. Hirahara, T. Aoki, T. Nagata, S. Igarashi and M. Yagi, *Polyhedron*, 2013, **52**, 455–460; (*b*) L. Yan, R. Zong and Y. Pushkar, *J. Catal.*, 2015, **330**, 255–260.

3 (*a*) J. E. Beves, E. C. Constable, S. Decurtins, E. L. Dunphy, C. E. Housecroft, T. D. Keene, M. Neuburger, S. Schaffner and J. A. Zampese, *CrystEngComm*, 2009, **11**, 2406–2416; (*b*) S. Hayami, Y. Komatsu, T. Shimizu, H. Kamihata and Y. H. Lee, *Coord. Chem. Rev.*, 2011, **255**, 1981–1990; (*c*) R. G. Miller and S. Brooker, *Inorg. Chem.*, 2015, **54**, 5398–5409.

4 (*a*) W.-W. Fu, F.-X. Zhang, D.-Z. Kuang, Y. Liu and Y.-Q. Yang, *J. Coord. Chem.*, 2015, **68**, 1177–1188; (*b*) T. Klemens, A. Świtlicka-Olszewska, B. Machura, M. Grucela, E. Schab-Balcerzak, K. Smolarek, S. Mackowski, A. Szlapa, S. Kula, S. Krompiec, P. Lodowski and A. Chrobok, *Dalton Trans.*, 2016, **45**, 1746–1762.

5 (*a*) C. M. A. Ollagnier, D. Nolan, C. M. Fitchett and S. M. Draper, *Supramol. Chem.*, 2012, **24**, 563–571; (*b*) J. R. Thompson, K. A. S. Goodman-Rendall and D. B. Leznoff, *Polyhedron*, 2016, **108**, 93–99; (*c*) C. Bai, B. Xu, H.-M. Hu, M.-L. Yang and G. Xue, *Polyhedron*, 2017, **124**, 1–11.

6 (*a*) G. Lowe, A. S. Droz, T. Vilaivan, G. W. Weaver, J. J. Park, J. M. Pratt, L. Tweedale and L. R. Kelland, *J. Med. Chem.*, 1999, **42**, 3167–3174; (*b*) S. Wang, W. Chu, Y. Wang, S. Liu, J. Zhang, S. Li, H. Wei, G. Zhou and X. Qin, *Appl. Organomet. Chem.*, 2013, **27**, 373–379; (*c*) G. Zhang, J. Tan, Y. Z. Zhang, C. Ta, S. Sanchez, S.-Y. Cheng, J. A. Golen and A. L. Rheingold, *Inorg. Chim. Acta*, 2015, **435**, 147–152; (*d*) W. Liu and R. Gust, *Coord. Chem. Rev.*, 2016, **329**, 191–213.

7 (*a*) S. Gama, I. Rodrigues, F. Marques, E. Palma, I. Correia, M. F. N. N. Carvalho, J. C. Pessoa, A. Cruz, S. Mendo, I. C. Santos, F. Mendes, I. Santos and A. Paulo, *RSC Adv.*, 2014, **4**, 61363–61377; (*b*) V. S. Stafford, K. Suntharalingam, A. Shivalingam, A. J. P. White, D. J. Mann and R. Vilar, *Dalton Trans.*, 2015, **44**, 3686–3700.

8 (*a*) M. N. Patel, H. N. Joshi and C. R. Patel, *J. Organomet. Chem.*, 2012, **701**, 8–16; (*b*) M. N. Patel, H. N. Joshi and C. R. Patel, *Polyhedron*, 2012, **40**, 159–167; (*c*) J.-W. Liang, Y. Wang, K.-J. Du, G.-Y. Li, R.-L. Guan, L.-N. Ji and H. Chao, *J. Inorg. Biochem.*, 2014, **141**, 17–27; (*d*) A. S. Mendo, S. Figueiredo, C. Roma-Rodrigues, P. A. Videira, Z. Ma, M. Diniz, M. Larguinho, P. M. Costa, J. C. Lima, A. J. L. Pombeiro, P. V. Baptista and A. R. Fernandes, *JBIC, J. Biol. Inorg. Chem.*, 2015, **20**, 935–948; (*e*) D.-Y. Zhang, Y. Nie, H. Sang, J.-J. Suo, Z.-J. Li, W. Gu, J.-L. Tian, X. Liu and S.-P. Yan, *Inorg. Chim. Acta*, 2017, **457**, 7–18.

9 (*a*) Z. Ma, L. Wei, E. C. B. A. Alegria, L. M. D. R. S. Martins, M. F. C. G. da Silva and A. J. L. Pombeiro, *Dalton Trans.*, 2014, **43**, 4048–4058; (*b*) G. Zhang, E. Liu, C. Yang, L. Li, J. A. Golen and A. L. Rheingold, *Eur. J. Inorg. Chem.*, 2015, **2015**, 939–947.

10 (*a*) C. R. Rice, C. J. Baylies, L. P. Harding, J. C. Jeffery, R. L. Paul and M. D. Ward, *Polyhedron*, 2003, **22**, 755–762; (*b*) J. D. Nobbs, A. K. Tomov, R. Cariou, V. C. Gibson, A. J. P. White and G. J. P. Britovsek, *Dalton Trans.*, 2012, **41**, 5949–5964; (*c*) G.-Y. Li, K.-J. Du, J.-Q. Wang, J.-W. Liang, J.-F. Kou, X.-J. Hou, L.-N. Ji and H. Chao, *J. Inorg. Biochem.*, 2013, **119**, 43–53; (*d*) L. Li, K. Du, Y. Wang, H. Jia, X. Hou, H. Chao and L. Ji, *Dalton Trans.*, 2013, **42**, 11576–11588; (*e*) K. Du, J. Liang, Y. Wang, J. Kou, C. Qian, L. Ji and H. Chao, *Dalton Trans.*, 2014, **43**, 17303–17316.

11 M. Manikandamathavan, V. Rajapandian, A. J. Freddy, T. Weyhermüller, V. Subramanian and B. U. Nair, *Eur. J. Med. Chem.*, 2012, **57**, 449–458.

12 (*a*) J. Wang and G. S. Hanan, *Synlett*, 2005, 1251–1254; (*b*) E. C. Constable, E. L. Dunphy, C. E. Housecroft, M. Neuburger, S. Schaffner, F. Schaper and S. R. Batten, *Dalton Trans.*, 2007, 4323–4332; (*c*) A. N. Kharat, A. Bakhoda and S. Zamanian, *Polyhedron*, 2011, **30**, 1134–1142.

13 G. Wilkinson, R. D. Gillard and J. A. McCleverty, *Comprehensive coordination chemistry: the synthesis, reactions, properties & applications of coordination compounds. Main group and early transition elements*, Pergamon Press, 1987.

14 A. W. Addison, T. N. Rao, J. Reedijk, J. van Rijn and G. C. Verschoor, *J. Chem. Soc., Dalton Trans.*, 1984, 1349–1356.

15 M. Llunell, D. Casanova, J. Cirera, P. Alemany and S. Alvarez, *SHAPE version 2.0*, Universitat de Barcelona, 2010.

16 (*a*) J. Cirera, E. Ruiz and S. Alvarez, *Organometallics*, 2005, **24**, 1556–1562; (*b*) D. Casanova, M. Llunell, P. Alemany and S. Alvarez, *Chem. – Eur. J.*, 2005, **11**, 1479–1494.

17 C. R. Groom, I. J. Bruno, M. P. Lightfoot and S. C. Ward, *Acta Crystallogr., Sect. B: Struct. Sci.*, 2016, **72**, 171–179.

18 A. B. P. Lever, *Inorganic electronic spectroscopy*, Elsevier, Amsterdam, 1986.

19 C. F. Macrae, I. J. Bruno, J. A. Chisholm, P. R. Edfinfton, P. McCabe, E. Pidcock, L. Rodríguez-Monge, R. Taylor, J. van de Streek and P. A. Wood, *J. Appl. Crystallogr.*, 2008, **41**, 466–470.

20 (*a*) M. Martins, P. V. Baptista, A. S. Mendo, C. Correia, P. Videira, A. S. Rodrigues, J. Muthukumaran, T. Santos-Silva, A. Silva, M. F. C. G. da Silva, J. Gigante, A. Duarte, M. Gajewska and A. R. Fernandes, *Mol. BioSyst.*, 2016, **12**, 1015–1023; (*b*) Z. Ma, B. Zhang, M. F. C. G. da Silva,

A. S. Mendo, J. Silva, P. V. Baptista, A. R. Fernandes and A. J. L. Pombeiro, *Dalton Trans.*, 2016, **45**, 5339–5355; (*c*) L. Bao, J. Wu, M. Dodson, E. M. R. de la Vega, Y. Ning, Z. Zhang, M. Yao, D. D. Zhang, C. Xu and X. Yi, *Mol. Carcinog.*, 2017, **56**, 1543–1553.

21 (*a*) S. A. O'Toole, B. L. Sheppard, E. P. J. McGuinness, N. C. Gleeson, M. Yoneda and J. Bonnar, *Cancer Detect. Prev.*, 2003, **27**, 47–54; (*b*) R. M. Martin, H. Leonhardt and M. C. Cardoso, *Cytometry, Part A*, 2005, **67**, 45–52; (*c*) P. Cao, X. Cai, W. Lu, F. Zhou and J. Huo, *Evid. Based Complement. Alternat. Med.*, 2011, **2011**, 1–9; (*d*) Y. Yan, J. C. Bian, L. X. Zhong, Y. Zhang, Y. Sun and Z. P. Liu, *Biomed. Environ. Sci.*, 2012, **25**, 172–181.

22 (*a*) I. S. MacPherson and M. E. P. Murphy, *Cell. Mol. Life Sci.*, 2007, **64**, 2887–2899; (*b*) J. Yoon and E. I. Solomon, *Coord. Chem. Rev.*, 2007, **251**, 379–400; (*c*) Q. Zhu, Y. Lian, S. Thyagarajan, S. E. Rokita, K. D. Karlin and N. V. Blough, *J. Am. Chem. Soc.*, 2008, **130**, 6304–6305; (*d*) M. Srnec, U. Ryde and L. Rulíšek, *Faraday Discuss.*, 2011, **148**, 41–53; (*e*) C. T. Lyons, T. Daniel and P. Stack, *Coord. Chem. Rev.*, 2013, **257**, 528–540; (*f*) L. Rulíšek and U. Ryde, *Coord. Chem. Rev.*, 2013, **257**, 445–458; (*g*) E. I. Solomon, D. E. Heppner, E. M. Johnston, J. W. Ginsbach, J. Cirera, M. Qayyum, M. T. Kieber-Emmons, C. H. Kjaergaard, R. G. Hadt and Li Tian, *Chem. Rev.*, 2014, **114**, 3659–3853.

23 (*a*) M. Sutradhar, E. C. B. A. Alegria, M. F. C. Guedes da Silva, L. M. D. R. S. Martins and A. J. L. Pombeiro, *Molecules*, 2016, **21**, 425; (*b*) L. Martins, R. Nasani, M. Saha, S. Mobin, S. Mukhopadhyay and A. Pombeiro, *Molecules*, 2015, **21**, 425; (*c*) M. Sutradhar, E. C. B. A. Alegria, T. R. Barman, M. F. C. Guedes da Silva, K. T. Mahmudov, F. I. Guseynov and A. J. L. Pombeiro, *Polyhedron*, 2016, **117**, 666–671; (*d*) T. F. S. Silva, B. G. M. Rocha, M. F. C. Guedes da Silva, L. M. D. R. S. Martins and A. J. L. Pombeiro, *New J. Chem.*, 2016, **40**, 528–537; (*e*) T. A. Fernandes, V. André, A. M. Kirillov and M. V. Kirillova, *J. Mol. Catal. A: Chem.*, 2017, **426**, 357–367; (*f*) O. V. Nesterova, D. S. Nesterov, A. Krogul-Sobczak, M. F. C. Guedes da Silva and A. J. L. Pombeiro, *J. Mol. Catal. A: Chem.*, 2017, **426**, 516–515; (*g*) E. A. Buvaylo, V. N. Kokozay, O. Y. Vassilyeva, B. W. Skelton, O. V. Nesterov and A. J. L. Pombeiro, *Inorg. Chem. Commun.*, 2017, **78**, 85–90; (*h*) M. V. Kirillova, P. Tome de Paiva, W. A. Carvalho, D. Mandelli and A. M. Kirillov, *Pure Appl. Chem.*, 2017, DOI: 10.1515/pac-2016-1012.

24 (*a*) W. Brackman and C. J. Gaasbeek, *Recueil*, 1966, **85**, 242–256; (*b*) A. M. Sakharov and I. P. Skibida, *Kinet. Catal.*, 1988, **29**, 102–107; (*c*) A. M. Sakharov and I. P. Skibida, *J. Mol. Catal.*, 1988, **48**, 157–174; (*d*) A. M. Sakharov and I. P. Skibida, in *New Developments in Selective Oxidation II*, ed. V. Cortes Corberan and S. V. Belion, Elsevier, 1994, pp. 629–637; (*e*) L. I. Simandi, *Catalytic Activation of Dioxygen by Metal Complexes*, Kluwer Academic Publishers, Dordrecht, 1992; (*f*) *The Activation of Dioxygen and Homogeneous Catalytic Oxidation*, ed. D. H. R. Barton, A. E. Martell and D. T. Sawyer, Plenum, New York, 1993; (*g*) I. E. Markó, P. R. Giles, M. Tsukazaki, I. Chellé-Regnaut, A. Gautier, S. M. Brown and C. J. Urch, *J. Org. Chem.*, 1999, **64**, 2433–2439; (*h*) H. Korpi, V. Sippola, I. Filpponen, J. Sipila, O. Krause, M. Leskela and T. Repo, *Appl. Catal., A*, 2006, **302**, 250–256; T. Punniyamurthy and L. Rout, *Coord. Chem. Rev.*, 2008, **252**, 134–154; (*i*) Z. Yin, G. Zhang, T. Phoenix, S. Zheng and J. C. Fettinger, *RSC Adv.*, 2015, **5**, 36156–36166.

25 (*a*) G. B. Shul'pin and A. N. Druzhinina, *React. Kinet. Catal. Lett.*, 1992, **47**, 207–211; (*b*) G. B. Shul'pin, *J. Mol. Catal. A: Chem.*, 2002, **189**, 39–66; (*c*) G. B. Shul'pin, *C. R. Chim.*, 2003, **6**, 163–178; (*d*) G. B. Shul'pin, *Mini-Rev. Org. Chem.*, 2009, **6**, 95–104; (*e*) G. B. Shul'pin, Y. N. Kozlov, L. S. Shul'pina, A. R. Kudinov and D. Mandelli, *Inorg. Chem.*, 2009, **48**, 10480–10482; (*f*) G. B. Shul'pin, Y. N. Kozlov, L. S. Shul'pina and P. V. Petrovskiy, *Appl. Organomet. Chem.*, 2010, **24**, 464–472; (*g*) G. B. Shul'pin, *Org. Biomol. Chem.*, 2010, **8**, 4217–4228; (*h*) G. B. Shul'pin, *Catalysts*, 2016, **6**, 50; (*i*) G. Olivo, O. Lanzalunga and S. Di Stefano, *Adv. Synth. Catal.*, 2016, **358**, 843–863; (*j*) I. Garcia-Bosch and M. A. Siegel, *Angew. Chem., Int. Ed.*, 2016, **128**, 13065–13068.

26 (*a*) G. B. Shul'pin, Y. N. Kozlov, G. V. Nizova, G. Süss-Fink, S. Stanislas, A. Kitaygorodskiy and V. S. Kulikova, *J. Chem. Soc., Perkin Trans. 2*, 2001, 1351–1371; (*b*) D. S. Nesterov, E. N. Chygorin, V. N. Kokozay, V. V. Bon, R. Boča, Y. N. Kozlov, L. S. Shul'pina, J. Jezierska, A. Ozarowski, A. J. L. Pombeiro and G. B. Shul'pin, *Inorg. Chem.*, 2012, **51**, 9110–9122; (*c*) I. Gryca, B. Machura, J. G. Małecki, L. S. Shul'pina, A. J. L. Pombeiro and G. B. Shul'pin, *Dalton Trans.*, 2014, **43**, 5759–5776; (*d*) I. Gryca, B. Machura, J. G. Małecki, J. Kusz, L. S. Shul'pina, N. S. Ikonnikov and G. B. Shul'pin, *Dalton Trans.*, 2016, **45**, 334–351; (*e*) I. Gryca, B. Machura, L. S. Shul'pina and G. B. Shul'pin, *Inorg. Chim. Acta*, 2017, **455**, 683–695; (*f*) A. I. Yalymov, A. N. Bilyachenko, M. M. Levitsky, A. A. Korlyukov, V. N. Khrustalev, L. S. Shul'pina, P. V. Dorovatovskii, M. A. Es'kova, F. Lamaty, X. Bantreil, B. Villemejeanne, J. Martinez, E. S. Shubina, Y. N. Kozlov and G. B. Shul'pin, *Catalysts*, 2017, **7**(4), 101; (*g*) A. N. Bilyachenko, A. N. Kulakova, M. M. Levitsky, A. A. Petrov, A. A. Korlyukov, L. S. Shul'pina, V. N. Khrustalev, P. V. Dorovatovskii, A. V. Vologzhanina, U. S. Tsareva, I. E. Golub, E. S. Gulyaeva, E. S. Shubina and G. B. Shul'pin, *Inorg. Chem.*, 2017, **56**, 4093–4103.

27 (*a*) A. Maroń, A. Szlapa, T. Klemens, S. Kula, B. Machura, S. Krompiec, J. G. Małecki, A. Świtlicka-Olszewska, K. Erfurt and A. Chrobok, *Org. Biomol. Chem.*, 2016, **14**, 3793–3808; (*b*) A. Maroń, S. Kula, A. Szlapa-Kula, A. Świtlicka, B. Machura, S. Krompiec, J. G. Małecki, R. Kruszyński, A. Chrobok, E. Schab-Balcerzak, S. Kotowicz, M. Siwy, K. Smolarek, S. Maćkowski, H. Janeczek and M. Libera, *Eur. J. Org. Chem.*, 2017, 2730–2745.

28 *Oxford Diffraction. CrysAlis PRO*, Oxford Diffraction Ltd, Yarnton, England, 2011.

29 G. M. Sheldrick, *SHELXS-97. Program for Crystal Structure Resolution*, Univ. of Göttingen, Göttingen, Germany, 1997.

30 O. A. Lenis-Rojas, A. R. Fernandes, C. Rodrigues, P. V. Baptista, F. M. Marques, D. Pérez-Fernández, J. Guerra, L. E. Sanchez, D. Vazquez-Garcia, M. Lopez-Torres, A. Fernández and J. J. Fernández, *Dalton Trans.*, 2016, **45**, 19127–19140.

31 (*a*) T. F. Silva, L. M. D. R. S. Martins, M. F. C. G. da Silva, A. R. Fernandes, A. Silva, P. M. Borralho, S. Santos, C. M. P. Rodrigues and A. J. L. Pombeiro, *Dalton Trans.*, 2012, **41**, 12888–12897; (*b*) A. Silva, D. Luis, S. Santos, J. Silva, A. S. Mendo, L. Coito, T. F. S. Silva, M. F. C. G. da Silva, L. M. D. R. S. Martins, A. J. Pombeiro, P. M. Borralho, C. M. Rodrigues, M. G. Cabral, P. A. Videira, C. Monteiro and A. F. Fernandes, *Drug Metab. Drug Interact.*, 2013, **28**, 167–176.